Dipolar Properties of and Temperature Effects on the Electronic States of 3-Hydroxyflavone (3HF) Determined using Stark-Effect Spectroscopy and Compared to Electronic Structure Calculations

Lavanya L. Premvardhan and Linda A. Peteanu*,†

Department of Chemistry, Carnegie Mellon University, Pittsburgh, Pennsylvania 15213

Received: March 17, 1999

3-Hydroxyflavone (3HF) is a molecule that undergoes excited-state intramolecular proton transfer (ESIPT). Using electroabsorption we have detected the small changes in dipole moment ($|\Delta\vec{\mu}|$) and polarizability ($\overline{\Delta\alpha}$) resulting from photon absorption for 3HF embedded in a noninteracting polyethylene environment. The values of $|\Delta\vec{\mu}|$ and $\overline{\Delta\alpha}$ obtained are also in good agreement with the results of ab initio 6-31G(2d,p) calculations but not with those obtained using INDO1/s. The electroabsorption spectra at 298 and at 77 K contain contributions from at least two overlapping electronic transitions within the wavelength region being probed. Two methods are discussed for extracting the electronic dipolar properties from these spectra that produce consistent results for the transition responsible for ESIPT. Interestingly, the relative intensities of the electroabsorption signals arising from the two electronic transitions studied here are observed to vary with temperature. The intensity change seen in the higher energy transition may be attributed to contributions from transition moment polarizability and hyperpolarizability components.

Introduction

3-Hydroxyflavone (3HF) is a model system for the study of excited-state intramolecular proton transfer (ESIPT) and is one of the first compounds in which this reaction was observed.[1] The dynamics of ESIPT has been extensively probed in a variety of solvents via steady-state and time-resolved spectroscopy.[1−23] In its ground state normal form (N), 3HF absorbs a photon to form N* which then undergoes ultrafast proton transfer[2−7] to produce the excited-state tautomer T*. The tautomer emits strongly Stokes-shifted fluorescence and has a long excited-state lifetime. Emission is followed by rapid ground-state reverse proton transfer from T to N.[7,8a] Due to these characteristic properties of ESIPT molecules, many are useful as laser dyes,[8,9] as UV stabilizers in polymers,[9,10] as fluorescence probes in biological systems,[11] and have the potential to be used as memory storage devices.[9,12]

One application that has received considerable attention of late is the development of fluorescence probes that exhibit a shift in absorption and/or emission energies that can be correlated with the polarity of the surroundings.[11,13] Typically, these shifts arise from the change in dipole moment and/or the change in polarizability of the electronic transition in question. For such probes to be effective, it is important that one can distinguish the effects of polarity on the spectrum of the probe from those resulting from acidity, basicity, or to rupture of the intramolecular hydrogen bond. Moreover, in order to efficiently screen the numerous available compounds for those most likely to exhibit the desired properties, it is useful to be able to rely on the results of quantum chemical calculations[24] and on the veracity of solvation corrections to the predicted values. For this purpose, detailed quantitative comparisons between condensed-phase experimental results and gas-phase calculations are of value.

In this work, electroabsorption (Stark-effect spectroscopy) is used to determine the change in dipolar properties, i.e., the dipole moment and polarizability changes, $|\Delta\vec{\mu}|$ and $\overline{\Delta\alpha}$, upon excitation (N → N*) of 3HF in a noninteracting low-density polyethylene (PE) environment. The PE matrix was chosen because it has been shown[14] not to disrupt the weak intramolecular hydrogen bond[2,15−17] of 3HF. In contrast, even hydrocarbon solvents must be dried thoroughly to avoid hydrogen bond scission.[2,15] Taken in conjunction with information regarding the change in dipole moment accompanying the tautomer fluorescence transition (T → T*) in ESIPT molecules,[18] these data shed light on the charge distribution of the excited state both prior to and following the proton-transfer reaction and can be used to verify quantum chemical models of these systems in the condensed phase. In this work, the measured values of $|\Delta\vec{\mu}|$ and $\overline{\Delta\alpha}$, and their projections along the transition moment ($|\hat{m}\cdot\Delta\vec{\mu}|$ and $\Delta\alpha_m$) for the N → N* transition, are found to compare well with the results of ab initio calculations but poorly with the predictions of INDO1/s. We argue that the latter discrepency is due to an improper description of the N* state. In contrast, there is good agreement between the INDO1/s, ab initio, and experimental results for both the ground state dipole moment and the excited state properties of higher lying electronic transitions.

A simple analysis of the solvatochromism of the N → N* absorption band of 3HF indicates that the solvation response of the ESIPT electronic transition of 3HF is not straightforward and may reflect interactions not accounted for by dielectric continuum theories. This is consistent with the findings of Catalán et al. who have determined that the correlation between the T → T* fluorescence transition wavelength and solvent polarity is also poor unless the basicity of the solvent is also taken into account.[13] They attribute this behavior to the fact that 3HF has a relatively weak intramolecular hydrogen bond and is therefore sensitive to the basicity of its environment. Stark

† E-mail: peteanu@andrew.cmu.edu.

10.1021/jp990933l CCC: $18.00
Published on Web 08/31/1999

spectroscopy is particularly well suited to the measurement of the dipolar properties of molecules such as 3HF that exhibit a complex solvent response.

Experimental Section

Sample. The sample consists of a piece of low-density PE film, into which the molecule of interest has been incorporated, sandwiched between two semitransparent inconel coated quartz electrodes. The sample film is prepared by immersion in a mM chloroform solution of 3HF for 5−15 min, lightly washed with chloroform to remove any excess sample adhered to the surface, then dried with a heat gun. The film is then heated between the inconel slides at 150 °C for ≈10 min. Typically, sample optical densities are between 0.2 and 0.6 at 342 nm, the room-temperature absorption maximum of 3HF.[26] A blank, needed to obtain the absorption spectrum, is prepared by the same procedure excluding the addition of 3HF to the chloroform solution. The thickness of the sample is determined from the interference patterns[27] in the near IR (900−2000 nm) using an absorption spectrometer (Perkin-Elmer λ900). Typical thicknesses of the PE films, determined by this method, are 50μ with an error of $\pm 1\mu$. The accuracy of this method had been verified with scanning electron microscopy measurements of a film of PE heated between two electrodes.

Solvent Studies. The absorption spectra of the probe molecules in μM concentrations were obtained in solvents of varying polarity. Non-hydrogen bonding solvents were chosen in order not to perturb the weak intramolecular hydrogen bond of 3HF. The absorption spectra of 3HF were obtained using distilled acetonitrile, and (Aldrich) anhydrous (≤0.005% H_2O) cyclohexane, 1,2-dichloroethane, and benzonitrile. All solvents were handled under nitrogen. The resolution of the absorption spectrometer (Perkin-Elmer λ900) is 0.25 nm.

Instrumentation. The broad band output of a 150W Xenon arc lamp (Oriel) is directed through a 0.3 m single grating Spex scanning monochromator. The output beam is passed through a quartz scrambler (CVI) and then through a Glan-Thomson polarizer to achieve horizontal polarization. A field of approximately 3.0 kV at 440 Hz is applied across the electrodes using a high voltage AC power supply (Joe Rolfe). By rotating the sample, the angle χ between the externally applied field and the polarization direction of the light beam is changed from 90° to 54.7°. In order to have the angle between the electric field and the electric field vector of the light beam effectively at 54.7°, which is the magic angle (see Analysis below), the external angle between the sample and the incoming light beam should be set at 60° at 298 K in order to correct for the refractive index change between air and PE and at 47° at 77 K to correct for the refractive index change between liquid nitrogen and PE. No correction is required for the quartz electrode interface, because the light beam both enters and exits this medium prior to passing through the PE sample. In all cases, spectra obtained at the magic angle will be referred to as $\chi = 54.7°$ though it should be noted that the above refractive index corrections have been made for the experimental measurements. The experiments were performed at a spectral resolution of 5 nm.

The voltage output from the silicon photodiode (UDT 0220UV) that detects the light transmitted by the sample is sent to a lockin detector (Stanford Research Systems 850). The output from the photodiode is split between an analog port that detects the total transmission (I), and the lockin port that detects the signal arising from field-induced modulation, ($\Delta I \approx 1 \times 10^{-5}$). The locked signal is detected at the second harmonic (2×440 Hz) of the applied field as the in-phase portion of the signal.

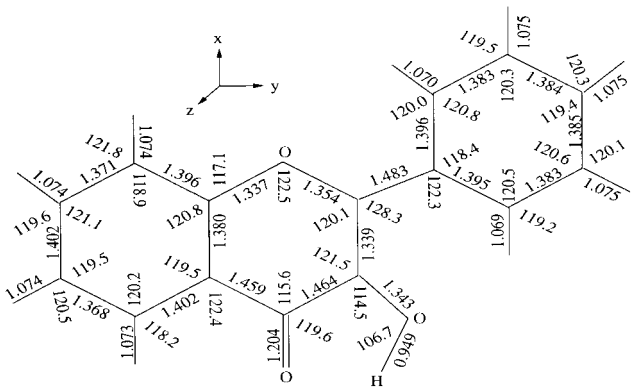

Figure 1. HF/6-31+G(2d,p) Geometry optimized bond lengths (Å) and bond angles of 3HF. The phenyl ring and hydroxychromone moiety are coplanar.

The monochromator and lockin detector are interfaced to a PC (Dell 386 MB) which employs Labwindows software to automate data collection. Electroabsorption spectra at 77 K are obtained using a HS Martin UV−vis liquid nitrogen immersion dewar.

Computations. Ab initio self-consistent field (SCF) calculations were performed using the Gaussian 94 package,[28] while semiempirical INDO1/s SCF calculations were performed with the quantum chemical electronic structure program, Argus.[29] The normal enol form of 3HF was geometry optimized using Hartree−Fock (HF) theory and the 6-31+G(2d,p) basis set. The 6-31G basis set is supplemented by the "+" diffuse and three polarization (two sets of d and one set of p) functions. The optimized structure of 3HF is planar and the bond lengths and bond angles are shown in Figure 1. The hydrogen-bond length in 3HF is 2.06 Å, indicating that it is weaker than that of other ESIPT systems we have studied.[25] Ground-state properties were determined from SCF calculations using HF/6-31G(2d,p) and INDO1/s. The excited state was modeled using single-excitation CI (configuration interaction) in both 6-31G(2d,p) and INDO1/s methods. Both the magnitude and the sign of the vectorial difference of the ground- and excited-state dipole moments, denoted as $\Delta\mu$, are reported. The ground- and excited-state polarizabilities were obtained from finite field (FF) calculations using an applied field of 0.001 au ($\approx 5 \times 10^6$ V/cm).[30]

Analysis

The formalism for electroabsorption developed by Liptay[31] is used to analyze the data. The change in absorption due to the application of an external electric field is fit to the weighted sum of zeroth, first, and second derivatives of the zero-field absorption spectrum. The absorption of the sample in eq 1 is expressed as the absorbance, $\epsilon(\nu)$, and is a function of the frequency ν:

$$\left(\frac{2\sqrt{2}}{\ln 10}\right)\frac{\Delta I}{I} = \Delta\epsilon(\nu) = \left[a_\chi \epsilon(\nu) + b_\chi \frac{\nu}{15h}\frac{\partial}{\partial\nu}\left(\frac{\epsilon(\nu)}{\nu}\right) + c_\chi \frac{\nu}{30h^2}\frac{\partial^2}{\partial\nu^2}\left(\frac{\epsilon(\nu)}{\nu}\right)\right]\vec{F}^2 \quad (1)$$

where $\vec{F}$ is the effective field at the site of the solute molecule. Experimentally, the change in transmitted light intensity ΔI, which is due to the application of an electric field, is measured and normalized by the total light intensity I reaching the detector. The $\Delta I/I$ term, measured as a root mean square voltage by the lockin amplifier, is multiplied by $2\sqrt{2}$ to convert it to an

equivalent dc voltage. The factor of ln 10 is derived from Beer's law as a change in intensity is measured here. The coefficients of the derivatives a_χ, b_χ, and c_χ depend on χ, the angle between the applied ac electric field vector and the electric field vector of the polarized light.

$$a_\chi = \frac{1}{30|\vec{m}|^2}\sum_{i,j}[10A_{ij}^2 + (3A_{ii}A_{jj} + 3A_{ij}A_{ji} - 2A_{ij}^2)(3\cos^2\chi - 1)] + \frac{1}{15|\vec{m}|^2}\sum_{ij}[10m_iB_{ijj} + (3m_iB_{jij} + 3m_iB_{jji} - 2m_iB_{ijj})(3\cos^2\chi - 1)] + \frac{\beta}{15|\vec{m}|^2}\sum_{ij}[10m_iA_{ij}\mu_{gj} + (3m_iA_{ji}\mu_{gj} + 3m_iA_{jj}\mu_{gi} - 2m_iA_{ij}\mu_{gj})(3\cos^2\chi - 1)] + \frac{\beta}{10}[\alpha_{gm} - \bar{\alpha}_g](3\cos^2\chi - 1) + \frac{\beta^2}{30}[3(\hat{m}\cdot\vec{\mu}_g)^2 - |\vec{\mu}_g|^2](3\cos^2\chi - 1) \quad (2)$$

$$b_\chi = \frac{1}{|\vec{m}|^2}\sum_{i,j}[10m_iA_{ij}\Delta\mu_j + (3m_iA_{ji}\Delta\mu_j + 3m_iA_{jj}\Delta\mu_i - 2m_iA_{ij}\Delta\mu_j)(3\cos^2\chi - 1)] + \frac{15}{2}\overline{\Delta\alpha} + \frac{3}{2}[\Delta\alpha_m - \overline{\Delta\alpha}](3\cos^2\chi - 1) + 5\beta(\vec{\mu}_g\cdot\Delta\vec{\mu}) + \beta[3(\hat{m}\cdot\vec{\mu}_g)(\hat{m}\cdot\Delta\vec{\mu}) - (\vec{\mu}_g\cdot\Delta\vec{\mu})](3\cos^2\chi - 1) \quad (3)$$

$$c_\chi = 5|\Delta\vec{\mu}|^2 + [3(\hat{m}\cdot\Delta\vec{\mu})^2 - |\Delta\vec{\mu}|^2](3\cos^2\chi - 1) \quad (4)$$

The ground state polarizability along the transition moment axis is α_{gm}, $\overline{\Delta\alpha}$ is the average polarizability ($Tr\Delta\alpha/3$), $\hat{m}$ is a unit vector in the direction of the transition moment, m_i is a component of the transition dipole moment, and $\beta = 1/kT$. Because the molecules are isotropically distributed in the PE matrix, only the magnitude of $\Delta\vec{\mu}$ is determined. In eqs 2 and 3, A and B are the transition moment polarizability and hyperpolarizability tensors, respectively. The effect of the field $\vec{F}$ at the site of the solute molecule, on the transition moment $\vec{m}$, is expressed as

$$\vec{m}(\vec{F}) = \vec{m} + A\cdot\vec{F} + B{:}\vec{F}^2 \quad (5)$$

At the magic angle ($\chi = 54.7°$) the b_χ and c_χ terms reduce to

$$b_{54.7} = \frac{10}{|\vec{m}|^2}\sum_{i,j}m_iA_{ij}\Delta\mu_j + 5\beta(\vec{\mu}_g\cdot\Delta\vec{\mu}) + \frac{15}{2}\overline{\Delta\alpha} \quad (6)$$

$$c_{54.7} = 5|\Delta\vec{\mu}|^2 \quad (7)$$

Note that three terms can contribute to $b_{54.7}$. The first term depends on A_{ij}, which is a component of the transition moment polarizability tensor. It reflects the magnitude of field-induced effects on the transition moment. For strongly allowed absorptions, such as the $\pi-\pi^*$ transitions studied here, this term is generally negligible relative to $\overline{\Delta\alpha}$ itself. Likewise, the second term in eq 6 may also be set to zero, even at room temperature, if the molecules in the polymer matrix are presumed to be in a random orientation and immobilized such that no reorientation of the molecule can be induced by the applied electric field.[32] This is presumed to be the case for 3HF in PE at 77K, but is not necessarily at 298 K, which is above the glass transition temperature of PE.[33]

The coefficients a_χ, b_χ, and c_χ are extracted by means of a linear least-squares (LLSQ) fit of the electroabsorption signal to the sum of derivatives of $\epsilon(\nu)$, using a program written in MATLAB (Mathworks). In the case of 3HF, the electroabsorption spectrum is poorly fit by a single set of a_χ, b_χ, and c_χ coefficients, indicating that the absorption spectrum of 3HF in the wavelength region 25000−35000 cm^{-1} consists of at least two overlapping electronic transitions. This fact is consistent with the response of the electroabsorption signal to changing the sample temperature and evidence from ab initio calculations and solvent absorption studies (see Results). In order to obtain the dipolar properties for both transitions, the LLSQ fit was performed using two different methods. In the first method, the spectrum was first separated into segments corresponding to the two electronic states and each segment was then fit separately. We have previously used a similar fitting method and obtained successful results.[25] The second method of fitting employs sums of gaussians to model the absorption spectrum (see Appendix).[34−37] The a_χ, b_χ, and c_χ parameters associated with each Gaussian can then be varied to obtain a fit to the electroabsorption spectrum. We find that this method gives results which are consistent with those obtained by separating the spectra into segments.

In both LLSQ fitting procedures used, the spacing between points was made uniform in frequency in order to obtain a better quality fit. The experimental data are uniformly spaced in wavelength. However, the direct conversion to frequency (cm^{-1}) results in a higher density of data points at lower frequencies and biases the LLSQ fit parameters in that region. Therefore, a cubic-spline interpolation function is used to generate data sets that are uniformly spaced in frequency. Prior to splining, the spectra are smoothed by using a sliding window mean[38] of the ordinate points, so that the derivatives of the smoothed absorption spectrum, obtained via numerical differentiation, are also smooth. After smoothing, the noise in each spectrum is less than ≈1% of the total signal, while prior to smoothing the noise varies from ≈1% at the red edge to ≈7% at the blue edge. The noise level is higher at the blue edge because of the lower power output of the lamp and the decreased sensitivity of the detector in the ultraviolet region. The results reported in Table 1 are the averages of six independent experimental determinations. Comparing the fit parameters derived before and after smoothing the spectra, the values of a_χ, b_χ, and c_χ do not change by more than 2% and the standard deviations of these parameters are nearly identical.

The enhancement of the applied external field at the site of the solute molecule $\vec{F}$ in eq 1 is the cavity field factor f. Here, calculated gas-phase values of $\Delta\mu$ and $\overline{\Delta\alpha}$ were scaled by this factor[31] to compare them to condensed-phase measurements. To best mimic the structure of 3HF, we have used an ellipsoid with three semiaxes $a_x > a_y > a_z$ to represent the molecular cavity.[39] The cavity field factor for an ellipsoid can be expressed as

$$f_i = \epsilon_0/(\epsilon_0 - A_i(\epsilon_0 - 1)) \quad (8)$$

where i is the x, y, or z axis.[40] The shape factor A, defined in terms of the semiaxes, a_x, a_y, and a_z, of the ellipsoid, can also be decomposed into diagonal components A_i integrated numerically over the dummy variable s

$$A_i = \frac{a_xa_ya_z}{2}\int_0^\infty \frac{ds}{(s + a_i^2)[(s + a_x^2)(s + a_y^2)(s + a_z^2)]^{1/2}} \quad (9)$$

TABLE 1: Calculated and Experimental Dipolar Properties of 3HF

3HF	$f \cdot \Delta\mu^{red}$	$\hat{m} \cdot \Delta\vec{\mu}^{red}$ (θ)	$f^2 \cdot \overline{\Delta\alpha}^{red}$	$f \cdot \alpha_m{}^{red}$	$f^2 \cdot \Delta\mu^{blue}$	$f^2 \cdot \overline{\Delta\alpha}^{blue}$
6-31G(2d,p)	2.16	2.01 (21°)	9.11		0.83	8.02
INDO/s	6.38	6.38 (0°)	33.34		1.75	14.92
[a]exptl 77 K	|1.84± 0.03|	|1.8 ± 0.4| (≈14°)	10.3± 0.6	30 ± 3	|1.4 ± 0.9|	1.4 ± 1
[b]exptl 77 K	|1.81± 0.02|		9.0 ± 0.5		|1.6 ± 0.1|	0.3 ± 2.0
[a]exptl 298 K	|1.64 ± 0.09|		2.3± 0.2		|1.6 ± 0.6|	36 ± 3
[b]exptl 298 K	|1.7 ± 0.2|		3 ± 1		|2.3± 0.7|	16 ± 1

[a] Results from segmented fit of the absorption spectrum. [b] Results from fit of the absorption spectrum to gaussians. Both fitting methods are described in the Results section. Dipole moments are in debye and polarizabilities in Å^3. The red and blue superscripts on these quantities refer to the corresponding low- and high-energy transitions, respectively (see text). Gas-phase calculated values of $\Delta\mu$ and $\overline{\Delta\alpha}$ are scaled by f and f^2, respectively, where f is the cavity field factor for an ellipsoidal cavity (see text). θ is the angle between the transition moment and difference dipole moment vectors.

The lengths of the semiaxes are chosen on the basis of the particle dimensions and the van der Waals radius of hydrogen (1.2 Å),[41] which is the lowest limit for the radius for a molecule on its edges.[39] The ellipsoidal cavity for 3HF has dimensions of $a_x = 6.8$ Å, $a_y = 4.4$ Å, and $a_z = 1.2$ Å. The cavity field correction was applied in the following manner. Because the dipole moment of the molecule lies in the *XY* plane, the *x* and *y* components of calculated gas-phase values of $\Delta\mu$ were multiplied by f_x and f_y respectively. Gas-phase values of $\overline{\Delta\alpha}$ were multiplied by the average of the sum of squares of f_x and f_y. As a result of this correction, the ab initio calculated values of $\Delta\mu$ and $\overline{\Delta\alpha}$ are increased by ≈5% and ≈13% (Table 1), respectively. The total field at the site of the solute molecule also includes a reaction field which depends on the ground- and excited-state dipolar properties of the probe molecules.[31] Surprisingly, we found that the deviation between the calculated and experimental values *increased* when we attempted to account for the reaction field using the standard corrections for an ellipsoidal cavity.[40] For example, the gas-phase calculated values of $\Delta\mu$ increased by an additional 15% and $\overline{\Delta\alpha}$ by an additional 55%. This correction was not performed on the results from our calculations presented here.

Results

The experimental electroabsorption spectra at $\chi = 54.7°$ and at $\chi = 90°$ are shown in Figures 2 and 3 respectively, with data obtained at low temperature (77 K) shown on the left and at room temperature (298 K) shown on the right. Each half of both figures has three panels. Panels a and b contain the absorption spectra. The absorption spectra of 3HF at 77 and 298 K have two maxima: a high-energy (blue) peak, ν_{max}^{blue}, at ≈32500 cm^{-1} and a low-energy (red) peak, ν_{max}^{red}, at ≈29100 cm^{-1}. These peaks arise from transitions to two separate electronic states. The red peak exhibits a lower energy shoulder at 27700 cm^{-1} arising from a vibronic progression. These assignments are consistent with results from our electronic structure calculations and solvent absorption studies, presented in the following section, as well as with electroabsorption results as outlined below. In 3HF, ESIPT is known to occur from the lower energy state.[15,42]

The center and bottom panels in Figures 2 and 3 contain the electroabsorption spectra, shown as solid lines, which have been normalized by the square of the applied field ((V/cm)^2). Note that at 77 K the magnitude of the electroabsorption signal arising from the blue band is nearly a factor of ten smaller than that from the red band (Figures 2c and 3c). However the reverse is true at room temperature (Figures 2d and 3d), where the blue electroabsorption signal is about twice as large as that of the red band. The difference in the magnitudes of the red and blue signals, coupled with their varying response to a lowering of the temperature, reflects the fact that each arises from a separate electronic state that has different dipolar properties.

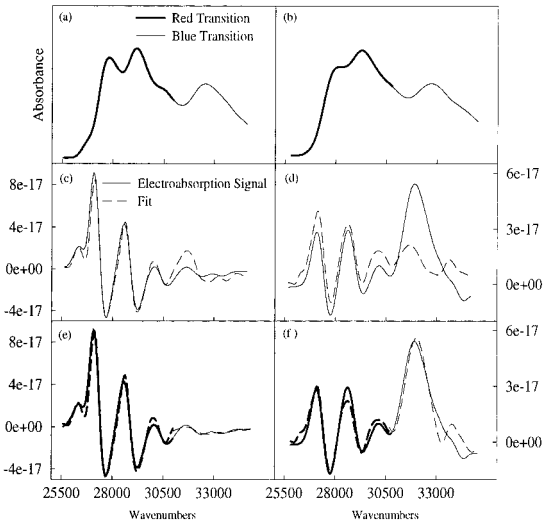

Figure 2. Spectra of 3HF at $\chi = 54.7°$. Absorption spectra at (a) 77 K and (b) 298 K. See text for definition of red and blue transitions. Electroabsorption spectrum (solid line) and fit (dashed line) to overall absorption spectrum at (c) 77 K and (d) 298 K. Electroabsorption spectrum (solid line) and segmented fit (dashed line) at (e) 77 K and (f) 298 K to the red (bold pen) and blue (normal pen) transitions described above. Results from the fits in e and f are reported in Table 1. The electroabsorption spectra have been normalized by the square of the applied field, and the *y*-axis units of c−f are in (cm/V)^2.

The LLSQ fits to the electroabsorption signal, which is the sum of the individual weighted derivatives (eq 1) of the absorption spectrum, are shown as dashed lines in the second and third panels. The fits to the overall electroabsorption signal, shown in panels c and d of Figures 2 and 3, are poor, particularly for room-temperature data (2d and 3d). This confirms that the dipolar properties are not uniform across this wavelength region. In order to extract the individual properties of each transition, the absorption spectrum was separated into two segments and fit in parts (panels e and f in Figures 2 and 3). The lower energy segment of the electroabsorption signal, shown in bold, was fit to the portion of the absorption spectrum that lies between 25500 and 31500 cm^{-1}, where 31500 cm^{-1} is approximately the valley between the two absorption maxima. The higher energy transition, shown with the lighter pen, was then fit to the portion of the absorption spectrum lying between 31500 and 35000 cm^{-1}. The limits which are used for the 77 K spectra are different than those used for the 298 K spectra because a better fit is obtained when the point of division of the room temperature absorption spectrum is at ≈30500 cm^{-1}. The difference in quality between the two methods of fitting is much more obvious at 298 K than at 77 K because the blue transition gives rise to

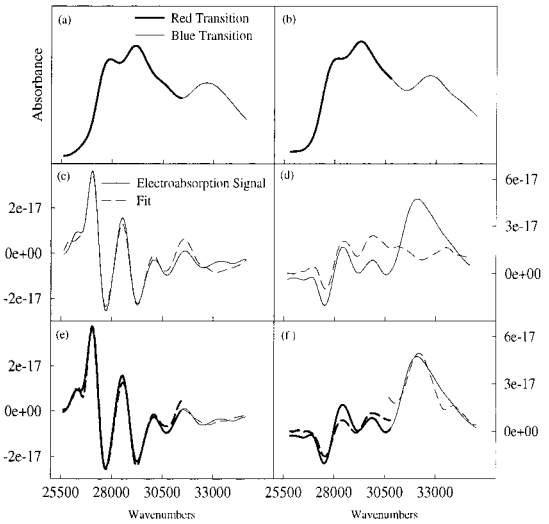

Figure 3. Spectra of 3HF at $\chi = 90°$. Absorption spectra at (a) 77 K and (b) 298 K. Electroabsorption spectrum (solid line) and fit (dashed line) to overall absorption spectrum at (c) 77 K and (d) 298 K. Electroabsorption spectrum (solid line) and segmented fit (dashed line) at (e) 77 K and (f) 298 K to the red (bold pen) and blue (normal pen) transitions described above. Results from the fits in e and f are reported in Table 1. The electroabsorption spectra have been normalized by the square of the applied field, and the *y*-axis units of c−f are in $(cm/V)^2$.

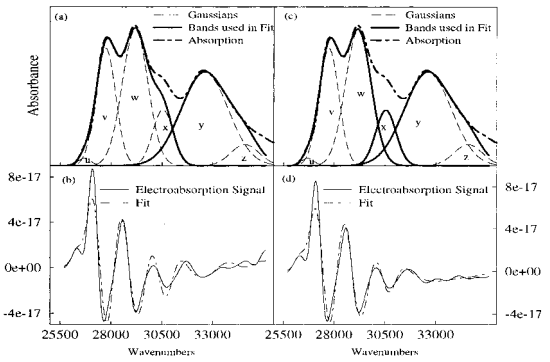

Figure 4. Fits for 3HF obtained using gaussians to fit the absorption spectrum at 77° K at $\chi = 54.7°$. (a) Absorption spectrum (bold dot−dash line), gaussians used to reproduce absorption (dashed line), two bands employed in fitting electroabsorption signal (bold solid lines). The red band is the sum of gaussians $u - x$ and the blue band is the sum of gaussians *y* and *z*. (b) Electroabsorption spectrum (solid line) and fit (dashed line) to the red and blue bands. Results from this fit are reported in Table 1. (c) Three bands used in fitting electroabsorption signal. Band 1 is the sum of gaussians $u - w$, band 2 is gaussian *x*, and band 3 is the sum of gaussians *y* and *z*. (d) Electroabsorption spectrum (solid line) and fit (dashed line) to bands 1, 2, and 3. The electroabsorption spectra have been normalized by the square of the applied field, and the *y*-axis units of b and d are in $(cm/V)^2$.

a distinctly larger signal at the higher temperature. The parameters derived from the analysis presented here are consistent with the results of ab initio calculations of $\Delta\mu$ and $\overline{\Delta\alpha}$ as described below (section Dipolar Properties) and summarized in Table 1 for the red and blue[43] bands.

An alternate method of fitting these overlapping transitions is to model the absorption spectrum to gaussians or sums of gaussians (Figures 4 and 5). A detailed description of our application of this method[34−37] is outlined in the Appendix. The absorption spectrum, modeled by gaussians, was fit to the electroabsorption signal at $\chi = 54.7°$ in two ways. The signal was first fit to two bands: the red band (sum of gaussians $u-x$ at 77 K in Figure 4a and $v-x$ at 298 K in Figure 5a) and the blue band (gaussians *y* and *z* in both figures). The electroabsorption spectrum, fit simultaneously to the two absorption bands with six free parameters (one set of a_χ, b_χ, and c_χ for each band), are shown in Figures 4b and 5b, and the results of these fits are reported in Table 1. Because of the poor quality of fit obtained for the room-temperature spectra when only two bands were used, a second fit was performed for which a third band was included (see Figures 4d and 5d and Appendix).

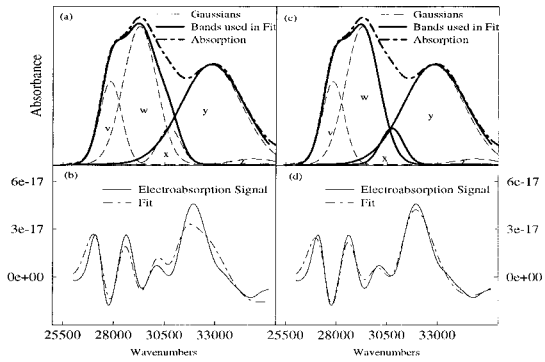

Figure 5. Fits to the 298 K electroabsorption spectrum of 3HF at $\chi = 54.7°$ using gaussians. As in Figure 4 two methods of fitting were used. (a) The absorption spectrum fit to two bands. Here the red band is the sum of gaussians $v-x$. (b) Fit to the electroabsorption signal using the bands shown in a. (c) The absorption spectrum fit to three bands. Here, band 1 is the sum of gaussians $v-w$. (d) Fit to the electroabsorption signal using the bands shown in c. The remaining bands in a and c are identical to those in Figure 4a and c, respectively. The electroabsorption spectra have been normalized by the square of the applied field, and the *y*-axis units of b and d are in $(cm/V)^2$. See Figure 4 for definitions of legends.

TABLE 2: Calculated and Experimental Transition Energies (in cm^{-1}) and Oscillator Strengths of 3HF[a]

3HF	$\nu^{red} \times 10^3$	f_{red}	$\nu^{blue} \times 10^3$	f_{blue}
6-31G(2d,p)	41.904	0.71	46.438	0.08
INDO1/s	32.139	0.65	34.876	0.04
polyethylene 77 K	27.7 ± 0.2	≈0.33	32.5 ± 0.2	≈0.22
polyethylene 298 K	28.1 ± 0.2	≈0.33	32.6 ± 0.2	≈0.22

[a] Experimental absorption peaks ν^{red} (the experimental values correspond to the low-energy shoulder of the absorption which is the 0-0 transition, see text) and ν^{blue} are reported in cm^{-1}. The corresponding oscillator strengths are compared to ab initio ($S_0 \rightarrow S_1$ and $S_0 \rightarrow S_3$) and INDO1/s ($S_0 \rightarrow S_2$ and $S_0 \rightarrow S_3$) calculations.

In light of the overall better quality of fits for the low-temperature spectra and the reduction in the influence of temperature-dependent factors on the derived parameters, we compare these low-temperature electroabsorption results to electronic structure calculations below.

Discussion

Assignment of Transitions. The electronic transition energies from the ground to the first four excited states ($S_0 \rightarrow S_1$ to $S_0 \rightarrow S_4$) were determined by both ab initio and INDO1/s methods (Table 2). Using INDO-based calculations, we and others[18,42] have obtained the result that the $S_0 \rightarrow S_1$ transition is of $n-\pi^*$ character. However, the red absorption band that is associated with ESIPT has a relatively large measured oscillator strength that is typical of a $\pi-\pi^*$ transition.[18] Therefore it is assigned to the $S_0 \rightarrow S_1$ transition in ab initio and the $S_0 \rightarrow S_2$ transition in INDO1/s which lies ≈7300 cm^{-1} higher in energy than the $n-\pi^*$ transition. These have calculated oscillator strengths of 0.71 and 0.65, respectively.[44] We assigned the blue transition observed experimentally to the first calculated higher-energy

transition having a nonzero oscillator strength. This is the $S_0 \rightarrow S_3$ in both ab initio and INDO1/s calculations. However, both methods greatly underestimate the oscillator strength of this transition relative to that of the red band (Table 2).

The ab initio calculated electronic energies for the $S_0 \rightarrow S_1$ and $S_0 \rightarrow S_3$ transitions for 3HF are quite high compared with the position of the experimental absorption maxima. There also appears to be a disagreement that is on the order of 1200 cm^{-1} between experiment and calculations with respect to the difference in energy between electronic states. The latter is surprising given that ab initio calculations in general overestimate transition energies[45] but usually predict energy difference quite well in proton-transfer systems.[46] However, if the shoulder at the red edge of the absorption profile ($\approx$27700 cm^{-1}) is assigned as the 0-0 band, consistent with prior work,[6,14,22] the experimental energy difference between the first and next excited state is indeed comparable to that predicted by ab initio calculations.[47] INDO1/s calculations, on the other hand, predict more accurate absolute values for the transition energies and an energy gap between the $S_0 \rightarrow S_1$ and $S_0 \rightarrow S_3$ transitions that is close to the observed energy separation between the absorption maxima.

Dipolar Properties. The dipolar properties predicted by electronic structure calculations for the lowest energy $\pi-\pi^*$ transition can be directly compared to those determined for the red transition (Table 1). The 6-31+G(2d,p) optimized structure of 3HF is planar (Figure 1), in close agreement with the X-ray crystal structure (reported in ref 22). In contrast, the published results of AM1 optimization[23,42] give a torsion angle between the phenyl and hydroxychromone moieties of $\approx$30°. NMR studies have correlated a decrease in planarity in ortho-substituted 3HF with a weakening of the intramolecular hydrogen bond[21] indicating that a planar conformer favors ESIPT and the observation of tautomer fluorescence. As we and others[14] have found that 3HF exhibits predominantly tautomer fluorescence in PE, we conclude that it is planar in this environment. However, we also find that the results of ab initio calculations of the dipolar properties of the nonplanar structure do not differ substantially from those obtained for the planar structure.

The method of fitting by truncating the absorption spectrum is justified when compared to the results obtained using gaussians to model the red and blue transitions of the absorption band of 3HF at 77K (Figure 4a and b). The simultaneous fit to the two bands, where a_χ, b_χ, and c_χ for both bands are determined from a single fit, produces results for the red band (Figure 4b) that are in close agreement with the fits produced by truncating the spectrum (see Table 1). The three band gaussian fit (Figure 4c and d) does not greatly alter the quality of fit nor affect the parameters extracted for the red band. This is not surprising as the size of the electroabsorption signal is small in the region corresponding to gaussian *x*, the extra band in the three-band fit. Moreover, there is little overlap of *x* with adjacent gaussians at 77 K (Figure 4d).

Comparing the results from the segmented fit of the electroabsorption spectra to those from ab initio calculations, we find that $\Delta\mu$ and $\overline{\Delta\alpha}$ for the first excited state of 3HF are in good agreement. The ab initio results are $\approx$ 15% larger than the experimental $|\Delta\vec{\mu}|$ and $\approx$ 13% smaller than the experimental $\overline{\Delta\alpha}$ measured at 77 K. The measured value for the polarizability along the transition moment axis $\Delta\alpha_m$ is approximately 3 times $\overline{\Delta\alpha}$, as expected (see Analysis section). The angle between the transition moment and the difference dipole moment (θ in Table 1) as determined from $|\hat{m}\cdot\Delta\vec{\mu}|$, is also in good agreement with ab initio results. Our results are also in reasonable agreement with recent B3LYP hybrid density functional calculations for μ_g and CIS calculations of μ_e using a 6-31G(d,p) basis set which yield a vectorial difference of the dipole moment of $\approx$2.3D.[13]

TABLE 3: Ground and Excited State Dipole Moments and Polarizabilities Determined from Electronic Structure Calculations

3HF	μ_g	μ_e^{red}	μ_e^{blue}	α_g	α_e^{red}	α_e^{blue}
6-31G(2d,p)	3.15	3.61	3.15	23.92	31.98	28.47
INDO1	3.83	6.95	5.40	20.00	48.55	32.77

[a] Dipole moments are in debye and polarizabilities in Å^3.

The good agreement that is obtained with ab initio results are in contrast with the results of INDO1/s calculations which yield $\Delta\mu$ and $\overline{\Delta\alpha}$ values that are a factor of four larger than experiment. We have found that INDO1/s calculations greatly overestimate $\Delta\mu$ and $\overline{\Delta\alpha}$ values for other proton-transfer molecules as well.[25,48] The discrepancy clearly arises in the estimation of the excited-state properties of the state from which proton transfer occurs. Note that the ground state dipolar properties μ_g and α_g, estimated from INDO1/s calculations, are comparable to ab initio results (Table 3), while the corresponding excited-state properties for the red transition are much larger than those obtained by ab initio methods. However, note that the properties for the higher excited state determined from INDO1/s are in much better agreement with ab initio calculations and with the experimental results. Therefore, we infer that ab initio calculations better describe the potential-energy surface of the proton-transfer state for which coupling to the adjacent tautomer excited state must be taken into account. As proton transfer in 3HF occurs on a femtosecond timescale,[3] strong electronic coupling between the N* and T* states is likely. We have obtained similar results in comparing INDO1/s and ab initio results for the $\pi-\pi^*$ transition of proton-transfer molecules versus non-proton-transfer analogs.[48]

Because the low-temperature electroabsorption signal of the blue band is extremely weak, the fit is of lower quality and the derived parameters should be interpreted more qualitatively. The small magnitude of the signal indicates that this transition has a smaller $|\Delta\vec{\mu}|$ and/or $\overline{\Delta\alpha}$ than does the lower energy transition which is consistent with the predictions of both ab initio and INDO1/s calculations (Table 1). Overall, the values of $|\Delta\vec{\mu}|$ and $\overline{\Delta\alpha}$ for the blue transition are in reasonable agreement with ab initio calculations for the dipolar properties of the $S_0 \rightarrow S_3$ transition.

Interpretation of Electroabsorption Results at 298 K. The electroabsorption results obtained at 298 K can be analyzed to obtain information about the relative response of both states to lowering the temperature. From the segmented fit (Figures 2 and 3), we obtain similar values of $|\Delta\vec{\mu}|$ at both 298 and 77 K for the red band. Again, the gaussian fit to the two bands at room temperature (Figure 5a and b) is in good agreement with the results for the red band from the segmented fit. Even though the gaussian fit for the blue band is not as good as the segmented fit, the results of the two agree quantitatively. In order to improve the fit in the blue region at 298 K, a third band was included in the fit (gaussian *x* in Figure 5c). This does indeed improve the fit; however, the results obtained for the dipolar properties are unrealistic and are therefore not reported.

The large value of $b_{54.7}$ at 298 K for the blue band from the segmented fit, assigned to $\overline{\Delta\alpha}$ in Table 1, does not agree with calculations and its tenfold decrease when the temperature is lowered to 77 K may be due to the following effects. As

TABLE 4: Absorption Maxima of 3HF in Solvent and Polymer Environments[a]

solvent	ϵ_0	$\nu_{max}^{red} \times 10^3$	$\Delta\nu_{hex}^{red} \times 10^3$	$\nu_{max}^{blue} \times 10^3$	$\Delta\nu_{hex}^{blue} \times 10^3$
cyclohexane	2.02	29.44 ± 0.02	0	32.87 ± 0.03	0
1,2-dichloroethane	10.2	29.20 ± 0.02	-0.24 ± 0.04	32.57 ± 0.03	-0.30 ± 0.06
benzonitrile	25.6	29.05 ± 0.02	-0.39 ± 0.04	32.44 ± 0.03	-0.43 ± 0.06
acetonitrile	37.5	29.52 ± 0.02	$+0.08 \pm 0.04$	32.92 ± 0.03	$+0.05 \pm 0.06$
polyethylene 77 K	$\approx$2.3	29.1 ± 0.2	-0.34 ± 0.22	32.5 ± 0.2	-0.37 ± 0.23
polyethylene 298 K	2.3	29.3 ± 0.2	-0.14 ± 0.22	32.6 ± 0.2	-0.27 ± 0.23

[a] ϵ_0 = Dielectric constant. All absorption maxima are reported in cm^{-1}. ν_{max}^{red} and ν_{max}^{blue} are the shifts of each band relative to that of hexane.

previously stated, the $b_{54.7}$ term can contain additional contributions from the orientational component β and the transition moment polarizability A_{ij} (eq 6). If, as previously stated, the molecules are assumed to be completely immobilized in a random orientation in PE at 77 K, the contribution from the terms in β should then be zero. However, the magnitude of their contribution depends on the product $\vec{\mu}_g \cdot \Delta\vec{\mu}$ if the molecules reorient in the applied field. This is assumed to be the case for 3HF in PE at 298 K which is above the glass transition temperture of the matrix. Ab initio calculations indicate that $\vec{\mu}_g \cdot \Delta\vec{\mu}$ is negative for the $S_0 \rightarrow S_1$ transition and is positive for the $S_0 \rightarrow S_3$ transition. This is consistent with our experimental results where, upon lowering the temperature, $\overline{\Delta\alpha}$ for the red band increases while $\overline{\Delta\alpha}$ for the blue band decreases. However, this alone would not explain the comparatively large temperature effect on the magnitude of the electroabsorption signal of the blue band. This suggests that there is an additional contribution to $\overline{\Delta\alpha}$ for the blue band from the transition moment polarizability term. This proposal is supported by comparison of the a_χ (eq 2) value, which reflects the change in magnitude of the transition moment due to an applied field,[31c] determined for the two transitions at room temperature. We find that the a_{90} term for the blue band (6.3×10^{-16} $(cm/V)^2$) is indeed a factor of 8 larger than that for the red band (8.1×10^{-17} $(cm/V)^2$), at room temperature. Also, ab initio calculations show that an applied field of 0.001 au ($\approx 5 \times 10^6$ V/cm) enhances the magnitude of the transition moment by $\approx$3% for the $S_0 \rightarrow S_1$ transition and by $\approx$10% for the $S_0 \rightarrow S_3$ transition. Thus, contributions from the transition moment polarizability and hyperpolarizability are also likely to be the source of the larger energy shifts observed for the blue band in the solvent absorption studies described below.

Comparison to Solvent Absorption Analysis. The positions of the low- and high-energy absorption maxima were determined in solvents of varying polarity (see dielectric constants, ϵ_0, Table 4) and the relative shifts in energy of the peaks in each solvent with respect to that in cyclohexane are reported ($\Delta\nu_{hex}^{red}$ and $\Delta\nu_{hex}^{blue}$ in Table 4). For each solvent studied, these shifts are not identical, consistent with the electroabsorption results that the corresponding states have different dipolar properties. The anomalous blue shift in acetonitrile has been previously seen by us for other proton-transfer molecules,[25] and we believe it to be due to specific solute-solvent interactions. Somewhat surprisingly, the absorption maxima, ν_{hex}^{red} in Table 4, at both 298 and 77 K in PE appear to be red shifted with respect to the ν_{max} of 3HF in a solvent with a similar dielectric constant, such as cyclohexane (Table 4). A similar red shift has been observed for ethyl pyrene in PE with respect to *n*-hexane and has been attributed to the PE medium having a much higher effective polarizability than *n*-hexane.[49] We also note that an anomalous red shift of $\approx$170 cm^{-1} has been observed for 3HF in a highly viscous alcohol such as octanol ($\eta = 9.13$cP) versus methanol ($\eta = 0.59$cP),[17] though the dielectric constant of methanol is a factor of three larger than that of octanol. These results suggest a possible effect of viscosity on the position of the absorption maximum of 3HF.

The solvent absorption analysis illustrates that, as the polarity of the solvent increases, there is a corresponding shift to lower energy of both absorption maxima. This indicates that the dipole moments and polarizabilities of both excited states are larger than that of the ground state. However, the larger shift exhibited by the higher energy band in the room-temperature spectra suggests that the higher electronic state may have a larger dipole moment and/or polarizability than that of the lower excited state. This result is in agreement with the electroabsorption results obtained at 298 K where the $b_{54.7}$ term, is found to be larger for the blue transition than for the red transition (eq 6). As we have previously shown, $\overline{\Delta\alpha}$ can make a significant contribution to the overall magnitude of the solvent shift[25] in systems where μ_g and $\Delta\mu$ are relatively small. Additional contributions may arise from the transition moment polarizabilities and hyperpolarizabilities as described above.

In the past, we have performed solvatochromic studies on other ESIPT molecules to determine the sign of $\Delta\mu$ which cannot be obtained by Stark spectroscopy on randomly oriented samples.[25] In these cases solvatochromic results were consistent with electroabsorption results and with the predictions of ab initio calculations. Here, we have obtained the absorption spectrum of 3HF in a few solvents primarily to demonstrate the different responses to polarity of the red and blue electronic states. In this small sampling, we find that the shifts of the absorption maxima are not linear with solvent polarity (Table 4), in agreement with Catalán et al. who have conducted an extensive solvatochromic study on 3HF.[13] These authors also find that the shift of the *emission* maximum of 3HF does not exhibit a linear trend as a function of solvent polarity. Rather this function must be augmented by a solvent basicity factor in order to obtain a good correlation with the shift in the emission maximum. These results imply that the dominant interactions between 3HF and the solvent are not well described by dielectric continuum theory and may have important implications for the applications of 3HF as a polarity probe. For molecules of this type, therefore, the power of Stark spectroscopy to determine accurate values of $|\Delta\vec{\mu}|$ and $\overline{\Delta\alpha}$ is clearly underscored.[52]

Conclusion

The dipolar properties, $|\Delta\vec{\mu}|$ and $\overline{\Delta\alpha}$ between the ground and excited states, of 3HF determined by electroabsorption studies are shown to be in good agreement with ab initio calculations but not with INDO1/s results. The overestimation of these values primarily in INDO1/s calculations may be due to a lack of a proper description of the excited state of the normal form because it is strongly coupled with the tautomer excited state. Moreover, analysis of the solvent shifts of the absorption spectra also yield inconsistent results in comparison with electroabsorption and ab initio calculations, suggesting that the interactions between 3HF and the solvent are not properly

accounted for by dielectric continuum theory and underscoring the power of Stark-effect spectroscopy to provide accurate dipolar properties for systems of this type.

Acknowledgment. We would like to thank our sources of funding: The Winters Foundation, the Petroleum Research Fund administered by the American Chemical Society, the NSF-RPG and CAREER programs, and the NSF-POWRE program. The Gaussian94 calculations were performed on Pentium II computers donated by Intel, Inc., as part of the "Technology for Education 2000" initiative. The authors acknowledge the Center for Molecular Analysis at Carnegie Mellon University for the use of the absorption spectrometer for the data collected for this research. We are also grateful to Dr. Andrew Shreve for useful suggestions, Dr. David Yaron for useful discussions regarding the use of gaussians in our analysis, Dr. Hyung J. Kim for useful discussions about solvation models, and Arindam Chowdhury for insightful suggestions about the low-temperature experiments.

Appendix

Fitting to Gaussians. When fitting electroabsorption signals, gaussians or sums of gaussians are routinely used as smoothing functions for noisy absorption spectra because the noise is enhanced when derivatives of the absorption spectra are taken. This method of analysis can also be exploited to extract dipolar properties of multiple overlapping electronic or vibronic states.[34−37] The absorption bandshape $\epsilon(\nu)$ can be represented by the sum of i gaussians where gaussian i centered at ν_c has height H and a full width at half-maximum (*fwhm*) of σ.

$$\epsilon(\nu) = \Sigma_i H_i \exp\frac{-(\nu - \nu_{c,i})^2}{2\sigma_i^2} \qquad (10)$$

A gaussian or a sum of gaussians can be used to model the overall absorption spectrum. The overall electroabsorption signal arising from electronic or vibronic states is a sum of the signals from each individual transition i.

$$\Delta\epsilon(\nu) = \Sigma_i \Delta\epsilon_i(\nu) \qquad (11)$$

The use of gaussians makes it possible to deconvolve the electroabsorption signal of each individual transition i from the overall measured signal.

The absorption spectrum of 3HF can be modeled with a minimum of four gaussians (v, w, x, and y in Figures 4 and 5). However, to reproduce additional features in the spectrum that are essential to fit the electroabsorption signal, gaussian z was included in both spectra and gaussian u in the low-temperature absorption spectrum. The lower energy transition is modeled with four gaussians ($u - x$), corresponding to a maximum ($\approx$29100 cm^{-1}) and two shoulders ($\approx$27700 cm^{-1} and $\approx$30100 cm^{-1}). The sum of these gaussians ($u - x$), which models the red absorption band, can be reproduced with a variety of differently parameterized gaussians. The gaussians for the red and blue bands in Figures 4a and 5a were summed together under the assumption that the underlying transitions (gaussians $u-x$) of a single electronic state (the red band) would have the same electrooptical properties. The higher energy transition can be modeled by two gaussians, (y and z in Figures 4 and 5), for which the parameters remain relatively fixed because y is the dominant gaussian, and does not significantly overlap[51] with gaussians w and x.

The method described above was used successfully to fit the 77 K absorption and Stark spectra of 3HF. Here the electroabsorption signal from the red band dominates the spectrum and the contribution from the blue band is small (Figure 4b). However, at 298K, the signal from the blue band is large and the two-band fit is not adequate to model the electroabsorption signal (Figure 5b). Therefore, it was necessary to add a third band to improve the fit. The three bands were chosen such that band 1 is the sum of gaussians $u-w$, band 2 is gaussian x, and band 3 is the sum of gaussians y and z. The simultaneous fit to three bands with nine free parameters is shown in Figures 4d and 5d. The three-band fit is indeed better at room temperature (Figure 5d) in comparison with the two-band fit (Figure 5b), especially in the blue region. Not surprisingly, this additional gaussian does not have a significant effect on the low-temperature fit as the magnitude of the electroabsorption signal is quite small in the blue region (compare Figures 4b and 4d). Unfortunately, though the fit at 298 K is improved, it yields the unphysical result that $|\Delta\vec{\mu}|$ and $\overline{\Delta\alpha}$ values for band 2 are much larger that that for band 3 which disagrees with the results of the segmented fit and the solvent shift studies.

In conclusion, we find this method is most successful if the region of overlap between transitions having different dipolar properties is small. This is found to be the case for 3HF, particularly at low temperature.

References and Notes

(1) Sengupta, P. K.; Kasha, M. *Chem. Phys. Lett.* **1979**, *68*, 382.
(2) McMorrow, D.; Dzugan, T. P.; Aartsma, T. J. *Chem. Phys. Lett.* **1984**, *103*, 492.
(3) Schwartz, B. J.; Peteanu, L. A.; Harris, C. B. *J. Phys. Chem.* **1992**, *96*, 3591.
(4) Ormson, S. M.; LeGourrierec, D.; Brown, R. G.; Foggi, P. *J. Chem. Soc., Chem. Commun.* **1995**, *20*, 2133.
(5) Ito, A.; Fujiwara, Y.; Itoh, M. *J. Chem. Phys.* **1992**, *96*, 7474.
(6) Brucker, G. A.; Swinney, T. C.; Kelley, D. F. *J. Phys. Chem.* **1991**, *95*, 3190.
(7) Brucker, G. A.; Kelley, D. F. *J. Phys. Chem* **1987**, *91*, 2856.
(8) (a) Chou, P.; McMorrow, D.; Aartsma, T. J.; Kasha, M. *J. Phys. Chem.* **1984**, *88*, 4596. (b) Parthenopoulos, D. A.; McMorrow, D.; Kasha, M. *J. Phys. Chem.* **1991**, *95*, 2668. (c) Chou, P.; Aartsma, T. J. *J. Phys. Chem.* **1986**, *90*, 721.
(9) Acuña, A. U.; Amat-Guerri, F.; Costela, A.; Douhal, A.; Figuera, J. M.; Florido, F.; Sastre, R. *Chem. Phys. Lett.* **1991**, *187*, 98.
(10) (a) Heller, H. J.; Blattmann, H. R. *Pure Appl. Chem.* **1973**, *36*, 141. (b) Tarkka, R. M.; Jenekhe, S. A. *Chem. Phys. Lett.* **1996**, *260*, 533.
(11) (a) Sytnik, A.; Gormin, D.; Kasha, M. *Proc. Natl. Acad. Sci. U.S.A.* **1994**, *91*, 11968. (b) Guharay, J.; Chaudhuri, R.; Chakrabarti, A.; Sengupta, P. K. *Spectrochim. Acta* **1997**, *53A*, 457. (c) Sarkar, M.; Guha Ray, J.; Sengupta, P. K. *Spectrochim. Acta* **1996**, *52A*, 275.
(12) Nishiya, T.; Yamauchi, S.; Hirota, N.; Baba, M.; Hanazaki, I. *J. Phys. Chem.* **1986**, *90*, 5730.
(13) Catalán, J.; Del Valle, J. C.; Díaz, C.; Palomar, J.; De Paz, J. L. G.; Kasha, M. *Int. J. Quantum Chem.* **1999**, *72*, 421.
(14) Mordzínski, A. *Chem. Phys. Lett.* **1988**, *152*, 151.
(15) McMorrow, D.; Kasha, M. *J. Phys. Chem.* **1984**, *88*, 2235.
(16) Barbara, P. F.; Walsh, P. K.; Brus, L. E. *J. Phys. Chem.* **1989**, *93*, 29.
(17) Standjord, A. J. G., Barbara, P. F. *J. Phys. Chem.* **1985**, *89*, 2355.
(18) Parthenopoulos, D. A.; Kasha, M. *Chem. Phys. Lett.* **1988**, *146*, 77.
(19) Woolfe, G. J.; Thistlethwaite, P. J. *J. Am. Chem. Soc.* **1981**, *103*, 6916.
(20) Swinney, T. C.; Kelley, D. F. *J. Chem. Phys.* **1993** *99*, 211.
(21) Standjord, A. J. G.; Smith, D. E.; Barbara, P. F. *J. Phys. Chem.* **1985**, *89*, 2362.
(22) Mühlfordt, A.; Bultmann, T.; Ernsting, N. P.; Dick, B. *Chem. Phys.* **1994**, *181*, 447.
(23) Cornard, J. P.; Vrielynck, L.; Merlin, J. C.; Wallet, J.C. *Spectrochim. Acta* **1995**, *51A*, 913.
(24) Kasha, M.; Parthenopoulos, D. A.; Dellinger, B. *Int. J. Quantum Chem.* **1993**, *45*, 689.
(25) Premvardhan, L.; Peteanu, L. *Chem. Phys. Lett.* **1998**, *296*, 521.
(26) In order to test for aggregation, we compared the absorption spectrum of 3HF in PE to that in cyclohexane and found no new features

that would be indicative of aggregation. The fluorescence excitation spectra of our 3HF sample in PE are also similar to those of Mordzínski[14] who also found no evidence for the aggregation of 3HF in PE.

(27) Seeger, K, *IEEE Trans. Microwave Theory Tech.* **1991**, *39*, 352.

(28) Frisch, M. J.; Trucks, G. W.; Schlegel, H. B.; Gill, P. M. W.; Johnson, B. G.; Robb, M. A.; Cheeseman, J. R.; Keith, T.; Petersson, G. A.; Montgomery, J. A.; Raghavachari, K.; Al-Laham, M. A.; Zakrzewski, V. G.; Ortiz, J. V.; Foresman, J. B.; Cioslowski, J.; Stefanov, B. B.; Nanayakkara, A.; Challacombe, M.; Peng, C. Y.; Ayala, P. Y.; Chen, W.; Wong, M. W.; Andres, J. L.; Replogle, E. S.; Gomperts, R.; Martin, R. L.; Fox, D. J.; Binkley, J. S.; Defrees, D. J.; Baker, J.; Stewart, J. P.; Head-Gordon, M.; Gonzalez, C.; Pople, J. A. *Gaussian94*, Revision E.2; Gaussian, Inc.: Pittsburgh, PA, 1995.

(29) Thompson, Mark A. Argus, Version 1.2, Richland, WA, 1992.

(30) Dykstra, C. E. *Chem. Rev.* **1993**, *93*, 2339.

(31) (a) Liptay, W. *Modern Quantum Chemistry, Part III: Action of Light and Organic Crystals;* Sinanoglu, O., Ed.; Academic Press: New York, 1965; p 45. (b) Liptay, W. *Excited States*; Lim, E. C., Ed.; Academic Press, New York, 1974; p 129. (c) Liptay, W. *Angew. Chem., Int. Ed.* **1969**, *8*, 177.

(32) Chowdhury, A.; Locknar, S.; Premvardhan, L.; Peteanu, L. Manuscript in preparation.

(33) Lide, D. R., Ed. *CRC Handbook of Chemistry and Physics*, 76th ed.; CRC Press, Inc.: Boca Raton, 1995.

(34) Wortmann, R.; Elich K.; Liptay, W. *Chem. Phys.* **1988**, *124*, 395.

(35) Pierce, D. W.; Boxer, S. G. *Biophys. J.* **1995**, *68*, 1583.

(36) Bublitz, G. U.; Boxer, S. G. *Annu. Rev. Phys. Chem.* **1997**, *48*, 213.

(37) Reimers, J. R.; Hush, N.S. *J. Phys. Chem.* **1991**, *95*, 9773.

(38) Press, W. H.; Flannery, B. P.; Teukolsky S. A.; Vetterling, W. T. *Numerical Recipes in C*; Cambridge University Press: Cambridge, 1988.

(39) Tomasi, J.; Persico, M. *Chem. Rev.* **1994** *94*, 2027.

(40) Bötthcher, C. J. F. *Theory of Electric Polarisation*; Elsevier Publishing Co.: Amsterdam, 1952.

(41) Bondi, A. *J. Phys. Chem.* **1964** *68*, 441.

(42) Dick, B. *J. Phys. Chem.* **1990** *94*, 5752.

(43) The quality of fit to the electroabsorption signal at 298 K with $\chi = 90°$ (Figure 3f) is poor. Therefore we have not reported the parameters with high standard deviations derived from this fit, which are $|\hat{m}\cdot\Delta\vec{\mu}|$ and $\Delta\alpha_m$.

(44) INDOs calculations on an AM1 optimized structure of 3HF gives an oscillator strength of 0.411 for the $\pi-\pi^*$ transition.[42]

(45) Vener, M. V.; Scheiner, S. *J. Phys. Chem.* **1995** *99*, 642.

(46) Matos, J. M. O.; Roos, B. O; Malmqvist, P-A. *J. Chem. Phys.* **1987**, *86*, 1458.

(47) The energy separation between the 0-0 and the 0-1 band also corresponds to a dominant mode in the Raman spectrum[23] at $\approx$1500 cm^{-1}.

(48) Peteanu, L.; Premvardhan, L. Manuscript in preparation.

(49) Zimerman, O. E.; Weiss, R. G. *J. Phys. Chem. A* **1998**, *102*, 5364.

(50) Lombardi, J. R. *J. Phys. Chem. A.* **1998**, *102*, 2817.

(51) One caveat is that extensively overlapped gaussians may result in nonunique solutions from the LLSQ routine used to fit the electroabsorption spectrum.